Biosensors and Bioelectronics 24 (2009) 1399–1404

Contents lists available at ScienceDirect

Biosensors and Bioelectronics

journal homepage: www.elsevier.com/locate/bios

High-throughput SPR sensor for food safety

Marek Piliarik, Lucie Párová, Jiří Homola*

Institute of Photonics and Electronics, Chaberská 57, 182 51 Prague, Czech Republic

ARTICLE INFO

Article history:
Received 25 May 2008
Received in revised form 25 July 2008
Accepted 5 August 2008
Available online 15 August 2008

Keywords:
Surface plasmon resonance
Biosensors
DNA chip
SPR imaging
Foodborne pathogens

ABSTRACT

High-throughput surface plasmon resonance (SPR) biosensor for rapid and parallelized detection of nucleic acids identifying specific bacterial pathogens is reported. The biosensor consists of a high-performance SPR imaging sensor with polarization contrast and internal referencing (refractive index resolution 2×10^{-7} RIU) and an array of DNA probes microspotted on the surface of the SPR sensor. It is demonstrated that short sequences of nucleic acids (20–23 bases) characteristic for bacterial pathogens such as *Brucella abortus*, *Escherichia coli*, and *Staphylococcus aureus* can be detected at 100 pM levels. Detection of specific DNA or RNA sequences can be performed in less than 15 min by the reported SPR sensor.

1. Introduction

Biosensors represent a promising technology for detection of chemical and biological analytes. In recent years, biosensors were increasingly used in numerous important applications such as medical diagnostics, environmental monitoring, food safety, and security (Farre et al., 2007). Current biosensors utilize optical, mechanical, or electrochemical transducers. Electrochemical sensors employ enzymes or other electrochemically active compounds to generate electrical signal (Palchetti and Mascini, 2008). Biosensors with mechanical transducers include microcantilevers and bulk or surface acoustic wave sensing devices (Lange et al., 2008; Sobel and Ballantine, 2008). Optical biosensors based on surface plasmon resonance (SPR) provide high sensitivity without the use of molecular labels. In addition, they show promise for development of high-throughput systems for parallelized measurements (Homola, 2008). The number of publications on SPR biosensors for detection of analytes implicated in food quality and safety has been growing (Lazcka et al., 2007; Patel, 2006). SPR biosensor-based detection of bacterial pathogens has been demonstrated employing immunoreactions between bacteria and specific antibodies immobilized on the SPR sensor surface (Oh et al., 2002; Taylor et al., 2006). Alternatively, bacterial pathogens can be measured by detecting their specific nucleic acids, such as rRNA sequences which can be extracted from bacterial pathogens (Nelson et al., 2002). This approach provides high specificity, stability and speed compared to antibody-based detection of whole bacteria (Wang et al., 2007). Furthermore, it takes advantage of the well-developed DNA array technology that is compatible with high-throughput operation format desired in many important applications (Boozer et al., 2006; Nelson et al., 2002). The most common approach to parallelized SPR sensing is SPR imaging (Rich and Myszka, 2006; Schaferling and Nagl, 2006; Wassaf et al., 2006). The main drawback of the SPR imaging is its rather limited refractive index resolution and limit of detection, which are typically one or two orders of magnitude worse than those provided by the best SPR sensors based on spectroscopy of surface plasmons (Nelson et al., 2001; Phillips and Cheng, 2007). Recently, an alternative approach to SPR imaging employing polarization control has been developed. The introduction of polarization control in SPR imaging has significantly improved both sensitivity and operating range, bringing the performance of SPR imaging sensors close to that of the best high-resolution sensors based on spectroscopy of surface plasmons (Piliarik and Homola, 2008; Piliarik et al., 2007).

In this paper, we combine a novel SPR biosensor platform based on SPR imaging with polarization contrast and internal referencing and a DNA array to provide a platform for detection of fragments of nucleic acids identifying DNA or RNA sequences specific for selected foodborne pathogens.

2. Materials and methods

2.1. Surface plasmon resonance imaging sensor

In this study, we use a novel self-referencing SPR imaging sensor with polarization contrast developed at the Institute of Photonics

* Corresponding author. Tel.: +420 266 773 448; fax: +420 284 680 222.
E-mail address: homola@ure.cas.cz (J. Homola).

0956-5663/$ – see front matter © 2008 Elsevier B.V. All rights reserved.
doi:10.1016/j.bios.2008.08.012

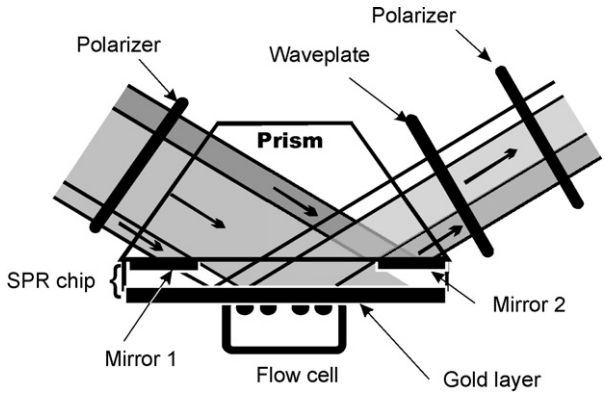

Fig. 1. Concept of SPR imaging with polarization contrast and internal referencing.

and Electronics (Piliarik and Homola, 2008). This sensor is based on the Kretschmann geometry of the attenuated total reflection method and prism coupling of light into a surface plasmon (Raether, 1988). In this configuration, the intensity and polarization of the reflected light depend on the coupling strength of the incident light beam to the surface plasmon. Therefore, a spatial distribution of refractive index changes can be correlated with a two-dimensional light intensity distribution as measured on a detector. A narrow-band light emitted by a superluminescent diode (central emission wavelength: 750 nm; full width at half maximum: 20 nm) is collimated and passed through a polarizer, a quarter-wave plate and made incident on the base of the coupling prism. Light reflected from the gold layer on the SPR chip interfaced with the prism is passed through another polarizer and imaged on a CCD camera. Telecentric imaging optics (Edmund optics GmbH, Germany) is used for the imaging to preserve array dimensions and avoid image distortion. Two gold mirrors are prepared on the prism surface and the SPR chip is attached directly to this surface via a refractive index matching fluid (Fig. 1). The light blocked and reflected by these mirrors provides dark and bright reference signals for real-time compensation for fluctuations in the dark current and intensity of incident light, respectively. Images acquired from the CCD camera are averaged (100 frames per record) and intensities from pixels within each measurement area are binned. The two polarizers and the wave-plate are set to extinguish the reflected light corresponding to a refractive index which is slightly lower than that of the used running buffer (Piliarik and Homola, 2008). Near this refractive index, a change in refractive index at the surface of the gold film results in a change in the polarization of reflected light and consequently in an increase in the intensity of transmitted light. An acrylic flow cell with gaskets made of 50-μm thick adhesive Mylar foil is pressed against the SPR chip to contain a liquid sample during the experiment. The gasket forms six flow chambers on the sensor surface, each containing a group of sensing channels. Each flow chamber is 0.9-mm wide. Length of the section of the flow chamber imaged on the CCD camera is 6.4 mm. A multichannel peristaltic pump is used to deliver six different samples simultaneously into the flow cell.

2.2. Refractive index calibration

In the refractometric experiment, a series of liquid samples with known refractive indices were sequentially flowed through the flow-cell. The samples were water solutions with different amounts of NaCl and their refractive indices were determined using a commercial refractometer (DSR-lambda, Schmidt Haensch GmbH, Germany). The samples were sequentially pumped through the flow-cell and incubated with the sensor surface until a stable baseline was established. One hundred and twenty measuring areas were defined in the image of the sensor surface and intensity was averaged across each area to yield output signal for each sensing channel. The output signal was normalized using the bright and dark signals reflected and blocked by the reference mirrors and the sensor output was calculated for each sensing channel in real time.

2.3. Selection of sequences

Five short DNA sequences were selected as a model system to represent specific fragments corresponding to RNA sequences from 16S ribosomal RNA of three different bacterial pathogens (*Brucella abortus*, *Escherichia coli*, and *Staphylococcus aureus*). The selected sequences are known to specifically identify these pathogens. 5′-(CGC TCC AGC CTA ACT GAA)-3′ (Herman and Deridder, 1992) and 5′-(TCC AGC CTA ACT GAA CCA TA)-3′ (Romero et al., 1995) are specific for *B. abortus*, 5′-(GTC CCC CTC TTT GGT CTT GC)-3′ (Nelson et al., 2002) and 5′-(TAT TAA CTT TAC TCC CTT CC)-3′ (Huijsdens et al., 2002) are specific for *E. coli*, and 5′-(CCT AAA AGG TTA CTC CAC CGG CT)-3′ (Greisen et al., 1994) is specific for *S. aureus*. The DNA targets were used instead of ribosomal RNA fragments mainly because of better stability of the DNA.

2.4. Reagents

Oligo(ethylene glycol) alkanethiol (OEG) (HS-C11-EG2-OH) was purchased from ProChimia Surfaces (Poland). Bovine serum albumin (BSA), tris buffer, phosphate buffered saline (PBS) (0.01 M phosphate, 0.137 M sodium chloride, 0.0027 M potassium chloride, pH 7.4), sodium chloride (NaCl) and magnesium chloride ($MgCl_2$) were purchased from Sigma–Aldrich (St. Louis, MO). Thiolated DNA sequences Bab970SH (5′-/5ThioMC6-D/CGC TCC AGC CTA ACT GAA-3′), Bab960SH (5′-/5ThioMC6-D/TCC AGC CTA ACT GAA CCA TA-3′), E441SH (5′-/5ThioMC6-D/TAT TAA CTT TAC TCC CTT CC-3′), E180SH (5′-/5ThioMC6-D/GTC CCC CTC TTT GGT CTT GC-3′) and Sau1463SH (5′-/5ThioMC6-D/CCT AAA AGG TTA CTC CAC CGG CT-3′) were purchased from Integrated DNA Technologies (Coralville, IA). Bab970SH and Bab960SH are specific to *B. abortus*, E441SH and E180SH are specific to *E. coli*, and Sau1463SH is specific to *S. aureus*. Complementary DNA sequences Bab970c (5′-TTC AGT TAG GCT GGA GCG-3′), Bab960c (5′-TAT GGT TCA GTT AGG CTG GA-3′), E441c (5′-GGA AGG GAG TAA AGT TAA TA-3′), E180c (5′-GCA AGA CCA AAG AGG GGG AC-3′), and Sau1463c (5′-AGC CGG TGG AGT AAC CTT TTA GG-3′) were purchased from Masaryk University (Brno, Czech Republic).

2.5. Preparation of SPR DNA chips

SPR sensor chips, made of BK7 glass (Schott, Inc., USA), were cleaned in a UV-ozone cleaner and coated with Ti adhesion layer (thickness ~1) and SPR active Au layer (thickness: 49.5 nm) by electron beam evaporation in vacuum. Coated chips were rinsed with absolute ethanol, deionized water and blown dry with nitrogen. Chips were then cleaned in a UV-ozone cleaner for 20 min, followed by rinsing with absolute ethanol and deionized water and dried with nitrogen stream. An array of sensing channels was prepared on the sensor surface by means of microspotting solution of 10-μM thiolated DNA probes in PBS. Commercial microarrayer OmniGrid (Genomic Solutions, USA) was used for the microspotting of sensing channels in such a way that the area corresponding to each flow chamber contained a series of channels with different DNA probes (three spots per sequence). Stealth pins (946MP9, TeleChem International, Inc., USA) with the tip dimensions approximately 300 μm × 300 μm and with an uptake channel for large arrays printing were utilized to create sensing channels of dimen-

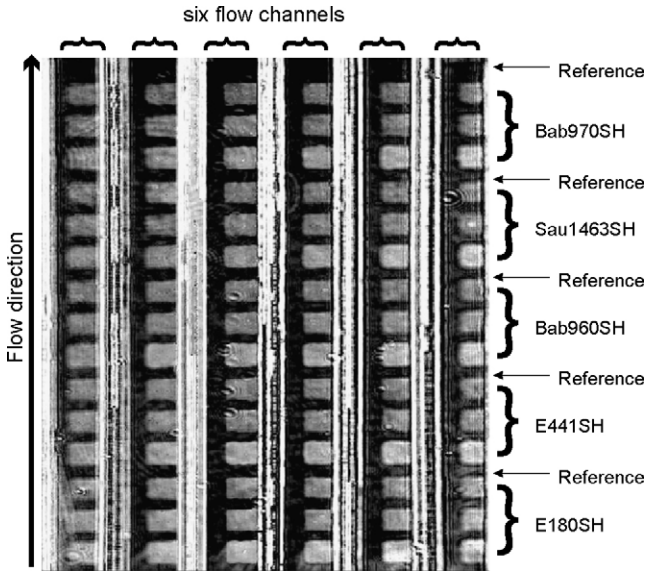

Fig. 2. Raw image generated in the SPR sensor with polarization contrast. Bright spots correspond to areas with the immobilized DNA probes. Flow-cell gaskets pressed against the SPR chip are shown as bright vertical strips.

sions 600 μm × 300 μm (a set of three, partly overlapping spots per channel were used). The microspotting took place in a humidity chamber with 90% humidity and after the spotting procedure the DNA spots were left in the chamber for additional 20 min before they were taken out. Then, the chips were rinsed with deionized water, blown dry with nitrogen and immersed over night in a solution of 100 μM OEG thiol in PBS. Before using a chip in the SPR imaging instrument, the chip was rinsed with deionized water and blown dry with nitrogen.

Fig. 2 shows a typical image obtained with the SPR imaging sensor. It shows six flow-chambers and a set of sensing channels represented by brighter rectangular areas. The difference in positions and geometry of microspotted channels on various chips was smaller than 20 μm, i.e. much smaller than the size of the sensing spots. Positions of rectangular areas in the SPR image corresponding to individual sensing channels were therefore maintained the same throughout all the experiments. It can be concluded that differences between SPR images of different microspotted chips influence SPR responses by less than 10%. Thirty reference channels (five in each flow-chamber) were defined in the areas of the image corresponding to the sensor surface coated with the non-fouling monolayer of self-assembled OEG thiols.

2.6. Detection of complementary oligonucleotides

In the detection experiments, the SPR imaging biosensor was combined with SPR chips containing five different DNA probes. One hundred and twenty measuring areas were defined in the image of the sensor surface (15 sensing channels and 5 reference channels in each flow-chamber) and intensity was averaged across each area to yield output signal for each sensing channel. The output signal was normalized using the bright and dark signals reflected and blocked by the reference mirrors, respectively, and the response was calculated in real time for each sensing channel. Sensor responses obtained from five reference channels within one flow-chamber were averaged and the resulting signal was subtracted from sensor responses obtained from 15 sensing channels in the same flow-chamber. This procedure allows compensating for changes in the background refractive index and temperature.

In order to characterize sensor response to each of the selected oligonucleotides, samples containing only a single oligonucleotide dissolved in TRIS buffer (10 mM tris, 30 mM $MgCl_2$) were characterized. First, TRIS buffer was flowed through the flow-cell for 5 min. Then, solutions containing oligonucleotides at various concentrations (0.2, 0.5, 1, 2, 5, 20 and 50 nM) were flowed through different chambers of the flow-cell for 15 min. Finally, the TRIS buffer was flowed through the flow-cell until a stable output signal was reached. The experiment was repeated for all selected oligonucleotides in different channels and on various SPR chips to obtain a set of 6–12 kinetics for each combination of oligonucleotide sequence and concentration.

3. Results and discussion

3.1. SPR imaging—refractometric calibration

In order to establish a bulk refractive index calibration for the SPR imaging sensor and to quantify its resolution, refractometric experiments were performed. The refractive index calibration obtained from this experiment is shown in Fig. 3a. The sensor response increases rapidly with the refractive index within the operating range (0.011 RIU). The corresponding change of normalized signal extends over almost two orders of magnitude and the sensitivity (derivative of the calibration curve) depends strongly

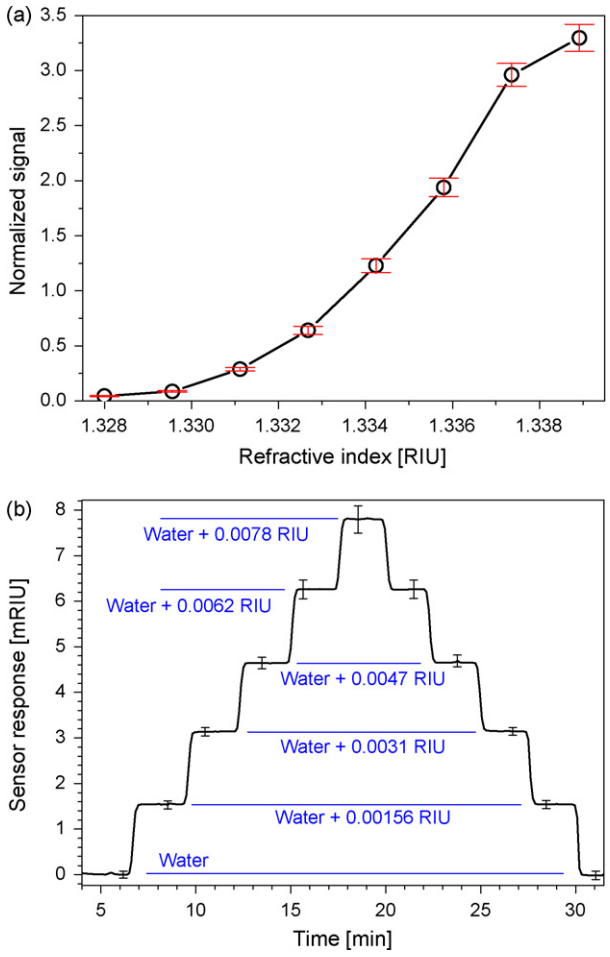

Fig. 3. Refractive index calibration curve (a) of the SPR imaging sensor response, and (b) linearized sensor response to a series of refractive index liquids recalibrated to 10^{-3} refractive index units (mRIU). Average response is plotted. Error bars indicate three standard deviations of the channel-to-channel variations.

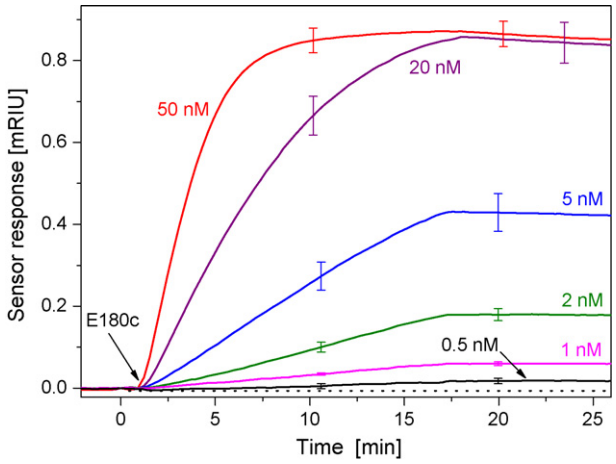

Fig. 4. Typical sensor responses to different concentrations of E180c oligonucleotides using the SPR imaging sensor with the microarray of sensing channels. Error-bars indicate three standard deviations.

on the normalized signal. Interpolated calibration curve (Ladd et al., 2008) was therefore used to compensate for non-linearity in the sensor response. Fig. 3b depicts temporal sensor response to sequential changes in the refractive index. The sensor response is expressed in 10^{-3} refractive index units (mRIU) using the calibration curve established earlier (Fig. 3a). Correlation of the sensor output with the actual refractive index of sample is quite high (the peak-to-peak difference is less than 7% for all 120 sensing channels). The capability of the sensor to resolve small changes in the refractive index is ultimately limited by the noise. The reported sensor exhibited standard deviation of the baseline noise below 10^{-6} RIU within the whole operating range (~0.011 RIU) and 2×10^{-7} RIU for the normalized signal close to one (Piliarik and Homola, 2008). This resolution is better by an order of magnitude than the resolution of other SPR imaging sensors reported to date.

3.2. Detection of individual oligonucleotides

In order to demonstrate the potential of the developed biosensor, a set of experiments, in which detection of oligonucleotides complementary to different probes immobilized on the sensor surface, was carried out. Synthetic target molecules were used to illustrate the instrumental performance of the SPR biosensor and its potential when the sensor is combined and operated in conjunction with appropriate technologies for processing of food samples and extraction of nucleic acids. As follows from Fig. 4, hybridization of target oligonucleotides with the probes on the SPR sensor surface produces a sensor response which depends on the concentration of target oligonucleotide. The equilibrium sensor response achieved with the highest concentration corresponds to saturation of the sensor surface. It can be shown that for the high affinity interaction (such as DNA hybridization with affinity constant $>10^8$ M^{-1}), all the accessible probes are hybridized in the saturation and the surface concentration of captured target molecules can be used to estimate their surface concentration. The surface concentration corresponding to the saturation signal can be calculated from the sensitivity of the SPR sensor as described previously in (Piliarik et al., 2007). The surface concentrations of accessible DNA probes microspotted on the surface were calculated to be 3.7×10^{12} DNA/cm^2 for Bab970SH, 5×10^{12} DNA/cm^2 for Bab960SH, 5.6×10^{12} DNA/cm^2 for Sau1463SH, 8.7×10^{12} DNA/cm^2 for E180SH, and 6.3×10^{12} DNA/cm^2 for E441SH. Although identical microspotting procedure was used for the functionalization of all the probes, the resulting concentrations of accessible oligonucleotide probes vary. However,

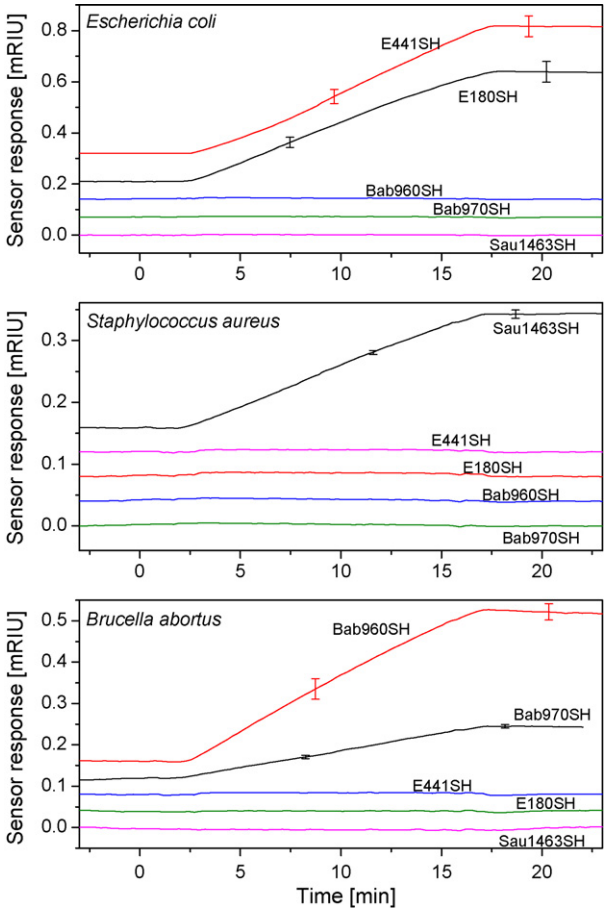

Fig. 5. Detection of oligonucleotide samples containing specific sequences of selected bacterial pathogens. Selected channels were functionalized with probes denoted at the detection kinetics in the graph.

the surface concentrations as well as the binding properties of the probes were close for different sensor chips and spotting runs. Average reproducibility was about 85%.

The operating range used for the detection of complementary oligonucleotides within one sensing channel is approximately 1 mRIU. However, measuring in all of the detection and reference channels simultaneously required a total operating range of about 3 mRIU. It is expected that for analysis of complex samples, even a wider operating range may be necessary.

As demonstrated in Fig. 5, the 5 nM concentrations of oligonucleotides specific for different pathogens (*B. abortus* mixture of Bab970c and Bab960c, *E. coli* mixture of E441c and E180c and *S. aureus* Sau1463c) induced a strong response in channels functionalized with the corresponding complementary probes. In the same experiment, amplitudes of responses in channels functionalized with probes corresponding to the other two pathogens were considerably lower (typically by a factor of 30–100) than the response in the specific channels. Moreover, the observed slight changes in the sensor response were likely mainly due to sample refractive index changes as follows from the kinetic behavior of the sensor response. This suggests that there is no significant cross-talk among the sensing channels and the functionalization procedure yields detection surfaces highly specific to each pathogen.

As the SPR biosensors measure hybridization kinetics, the sensor response was defined as the binding rate of the target to the probes in an initial phase of the binding experiment. The binding rates were calculated using a linear regression applied to the longest portion of

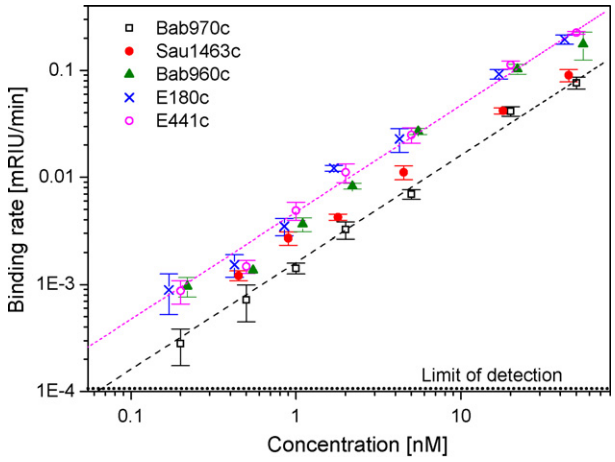

Fig. 6. Calibration curves for selected target oligonucleotides. Error bars indicate thee standard deviations of the experimental error. Overlapping data points are shifted on the *x*-axis by ±10% for better readability (oligonucleotide concentrations 200 pM, 500 pM, 1 nM, 2 nM, 5 nM, 20 nM and 50 nM). The lowest (Bab970c) and the highest (E441c) curves are fitted linearly through zero.

the kinetic sensor response fulfilling the criterion that the standard deviation of the linear fit was smaller than five standard deviations of the baseline noise. This method was applied automatically to all measured kinetics (using a MATLAB script) and the calculated binding rates for different concentrations of oligonucleotides are shown in Fig. 6. Calibration curves were determined using approximately 500 kinetic data sets acquired from various SPR chips and sensing channels. The observed differences in the binding rates of individual oligonucleotides are influenced by two factors: (i) the affinity of the complex (as well as the association rate constant) depends on the length and sequence of the oligonucleotides, and (ii) the binding rate depends strongly on the surface concentration of immobilized probes (in case that the mass transport is neglected this dependence is linear) which vary from sequence to sequence as calculated above. Although the concentration dependence of the sensor response is theoretically linear, at low concentrations, the rate of hybridization may be affected by mass transport. This effect is more significant in channels with higher surface coverage of accessible probes (particularly for *E. coli* sequences E180c and E441c). The channel-to-channel reproducibility measured within one chip is typically 95% (for concentrations above 1 nM) and the chip-to-chip reproducibility was found to be better than 85% which basically corresponds to the reproducibility of the functionalization. Furthermore, redundancy of sensing channels (three channels per each probe within each of the flow chambers) improves reliability of the measurements.

Clearly, the sensor shows a strong response even for target oligonucleotides at sub-nM concentrations. The minimum concentration measured in this work was 200 pM and the sensor response was distinguishable with typical channel to channel variation of ±30%. The limit of detection (LOD) is defined as a concentration of analyte that results in the sensor response equal to three standard deviations of the baseline noise (Thomsen et al., 2003). The lowest resolvable binding rate is therefore below 10^{-4} mRIU/min for 10 min detection run. The LOD was determined to be better than 60 pM for all tested oligonucleotides.

The achieved LOD is comparable or better than the detection limits for DNA reported using other biosensor technologies (Sassolas et al., 2008), such as electrochemical sensors (LOD in the range of 0.1–10 nM) (Fu et al., 2006; Kerman et al., 2003; Reisberg et al., 2008), surface acoustic wave sensors (LOD in the nM range) (Gronewold et al., 2006) or quartz crystal microbalance sensors (LOD in the 10–100 nM range; without amplification) (Uludag et al., 2008). The reported detection limit is also better than the best LODs obtained using high-performance SPR sensors based on spectroscopy of surface plasmons (Persson et al., 1997; Vaisocherová et al., 2006).

4. Conclusions

A high-throughput SPR sensor with polarization contrast and internal referencing was developed and applied to detection of oligonucleotides with sequences identifying specific foodborne bacterial pathogens. It was demonstrated that the reported sensor provides more than one order or magnitude better resolution (2×10^{-7} RIU) than the SPR imaging systems reported to date. The sensor was combined with microspotting for spatially resolved functionalization of the sensor with oligonucleotide probes. An array of oligonucleotide probes complementary to specific sequences of 16 S ribosomal RNAs of selected foodborne pathogens (*B. abortus*, *E. coli*, and *S. aureus*) was developed and used for detection of oligonucleotides with sequences identifying those pathogens. It was demonstrated that the target oligonucleotides can be detected at 100 pM level in less than 15 min.

Acknowledgements

This research was supported by the Academy of Sciences of the Czech Republic under the contract KAN200670701 and by the European Commission under the contract COLL-CT-2006-30392 (PATHOMILK).

References

Boozer, C., Kim, G., Cong, S.X., Guan, H.W., Londergan, T., 2006. Curr. Opin. Biotechnol. 17 (4), 400–405.
Farre, M., Kantiani, L., Barcelo, D., 2007. Trac-Trends Anal. Chem. 26 (11), 1100–1112.
Fu, Y.Z., Yuan, R., Chai, Y.Q., Zhou, L., Zhang, Y., 2006. Anal. Lett. 39 (3), 467–482.
Greisen, K., Loeffelholz, M., Purohit, A., Leong, D., 1994. J. Clin. Microbiol. 32 (2), 335–351.
Gronewold, T.M.A., Baumgartner, A., Quandt, E., Famulok, M., 2006. Anal. Chem. 78 (14), 4865–4871.
Herman, L., Deridder, H., 1992. Appl. Environ. Microbiol. 58 (6), 2099–2101.
Homola, J., 2008. Chem. Rev. 108 (2), 462–493.
Huijsdens, X.W., Linskens, R.K., Mak, M.T., Meuwissen, S.G.M., Vandenbroucke-Grauls, C.M.J.E., Savelkoul, P.H.M., 2002. J. Clin. Microbiol. 40 (12), 4423–4427.
Kerman, K., Morita, Y., Takamura, Y., Tamiya, E., 2003. Electrochem. Commun. 5 (10), 887–891.
Ladd, J., Taylor, A., Piliarik, M., Homola, J., Jiang, S., 2008. Anal. Chem. 80 (11), 4231–4236.
Lange, K., Rapp, B.E., Rapp, M., 2008. Anal. Bioanal. Chem. 391 (5), 1509–1519.
Lazcka, O., Campo, F.J.D., Munoz, F.X., 2007. Biosens. Bioelectron. 22 (7), 1205–1217.
Nelson, B.P., Grimsrud, T.E., Liles, M.R., Goodman, R.M., Corn, R.M., 2001. Anal. Chem. 73 (1), 1–7.
Nelson, B.P., Liles, M.R., Frederick, K.B., Corn, R.M., Goodman, R.M., 2002. Environ. Microbiol. 4 (11), 735–743.
Oh, B.K., Kim, Y.K., Bae, Y.M., Lee, W.H., Choi, J.W., 2002. J. Microbiol. Biotechnol. 12 (5), 780–786.
Palchetti, I., Mascini, M., 2008. Anal. Bioanal. Chem. 391 (2), 455–471.
Patel, P.D., 2006. J. AOAC Int. 89 (3), 805–818.
Persson, B., Stenhag, K., Nilsson, P., Larsson, A., Uhlen, M., Nygren, P.A., 1997. Anal. Biochem. 246 (1), 34–44.
Phillips, K.S., Cheng, Q., 2007. Anal. Bioanal. Chem. 387 (5), 1831–1840.
Piliarik, M., Homola, J., 2008. Sens. Actuat. B Chem. 134 (2), 353–355.
Piliarik, M., Vaisocherová, H., Homola, J., 2007. Sens. Actuat. B Chem. 121 (1), 187–193.
Raether, H., 1988. Spring. Tracts Modern Phys. 111, 1–133.
Reisberg, S., Dang, L.A., Nguyen, Q.A., Piro, B., Noel, V., Nielsen, P.E., Le, L.A., Pham, M.C., 2008. Talanta 76 (1), 206–210.
Rich, R.L., Myszka, D.G., 2006. J. Mol. Recogn. 19 (6), 478–534.
Romero, C., Gamazo, C., Pardo, M., Lopezgoni, I., 1995. J. Clin. Microbiol. 33 (3), 615–617.
Sassolas, A., Leca-Bouvier, B.D., Blum, L.J., 2008. Chem. Rev. 108 (1), 109–139.

Schaferling, M., Nagl, S., 2006. Anal. Bioanal. Chem. 385 (3), 500–517.
Sobel, R.M., Ballantine, D.S., 2008. Anal. Chim. Acta 608 (1), 79–85.
Taylor, A.D., Ladd, J., Yu, Q.M., Chen, S.F., Homola, J., Jiang, S.Y., 2006. Biosens. Bioelectr. 22 (5), 752–758.
Thomsen, V., Schatzlein, D., Mercuro, D., 2003. Spectroscopy 18 (12), 112–114.
Uludag, Y., Li, X., Coleman, H., Efstathiou, S., Cooper, M.A., 2008. Analyst 133 (1), 52–57.
Vaisocherová, H., Zítová, A., Lachmanová, M., Štěpánek, J., Králíková, Š., Liboska, Rejman, D., Rosenberg, I., Homola, J., 2006. Biopolymers 82 (4), 394–398.
Wang, X.W., Zhang, L., Jin, L.Q., Jin, M., Shen, Z.Q., An, S., Chao, F.H., Li, J.W., 2007. Appl. Microbiol. Biotechnol. 76 (1), 225–233.
Wassaf, D., Kuang, G.N., Kopacz, K., Wu, Q.L., Nguyen, Q., Toews, M., Cosic, J., Jacques, J., Wiltshire, S., Lambert, J., Pazmany, C.C., Hogan, S., Ladner, R.C., Nixon, A.E., Sexton, D.J., 2006. Anal. Biochem. 351 (2), 241–253.